Data analysis: Finding superheavy elements

K.J. Cook, L.T. Bezzina

October 20, 2017

1 Introduction

How are new elements discovered? In this workshop, we will analyse data from an experiment to find candidate nuclear reactions to form new superheavy elements. These nuclear reactions take place in femtometers (10^{-15} m) and take only zeptoseconds (10^{-21} s). You will learn how you can use simple physics principles together with cleverly designed experiments to gain deep insights into these physics processes that are otherwise inaccessible. In doing so, you will gain skills in multi-variable analysis that you will be able to apply to your own research.

This document is designed to give you some theoretical background in nuclear reactions, as well as an insight into one experimental approach to measuring nuclear reactions, before the workshop. If you've done a course in nuclear physics, many of these concepts will be familiar to you. In that case, please consider this a refresher.

2 Nuclear reactions

The positively charged centre of an atom – the atomic nucleus – is composed of protons and neutrons. When two nuclei collide in a nuclear reaction, two fundamental forces are relevant – the long-range Coulomb force, repelling the nuclei, and the short-range attractive strong (nuclear) force. These interactions can be described by the internuclear potential, shown schematically in Fig. 1. At large distances r, the Coulomb interaction dominates the nuclear potential. When the nuclei become close enough to almost touch $r \sim r_B$, the nuclear force begins to play a role, forming a local maximum V_B in the internuclear potential. This is known as the Coulomb barrier.

Depending on the trajectory of the colliding nuclei, and their total kinetic energy, two different things can occur:

1. The repulsive Coulomb force can cause the two nuclei to be diverted from their collision path. These nuclei may end up in an excited state as a result of this interaction, but they never get close enough to touch.

2. The two nuclei have close enough trajectories and sufficient kinetic energy to overcome the Coulomb force. In this case, they get close enough for the strong force to take effect. When this happens, **nuclear reactions** occur, resulting in changes in the compositions of the colliding nuclei (i.e. number of protons or neutrons). The degree of change depends mainly on how close the nuclei get. When the nuclei get very close, nuclear fusion can occur. In a purely classical picture (which we will be sticking with for this workshop), a projectile nucleus needs an energy equivalent to V_B to overcome the barrier and fuse with the target nucleus.

It is important to note that in any given experiment, all trajectories are sampled – from a head on collision to one where the nuclei pass so far away that their trajectories are not disturbed. Therefore, all possible nuclear reaction outcomes (depending on the energy and projectile-target combination) will occur. This means that while you may be only interested in on reaction outcome (say, fusion), you typically cannot study this outcome in isolation. Indeed, different reaction outcomes may compete with each other – this becomes important when producing new elements.

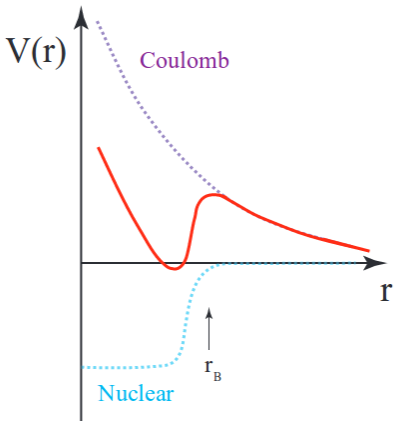

Figure 1: A sketch of the nuclear potential (red line) plotted as a function of internuclear separation r. This potential is the sum of the repulsive Coulomb potential (purple dots) and the attractive nuclear potential (blue dots)

3 Fusion: Forming new superheavy elements

The way we produce new superheavy elements is through nuclear fusion. For example, element 114, Flerovium, was first produced at JINR in Russia by the reaction

$$^{48}_{20}\mathrm{Ca} + ^{244}_{94}\mathrm{Pu} \rightarrow ^{292}_{114}\mathrm{Fl}^{*} \tag{1}$$

That's a $^{48}_{20}$Ca beam colliding with a $^{244}_{94}$Pu target to produce $^{292}_{114}$Fl in an excited state (indicated by the *). Element 118, Oganesson, was first produced at JINR in Russia (in collaboration with Lawrence Livermore National Laboratory) by

$$^{48}_{20}\mathrm{Ca} + ^{249}_{98}\mathrm{Cf} \rightarrow ^{297}_{118}\mathrm{Og}^{*} \tag{2}$$

Oganesson is the heaviest element to be produced so far. The race is now on to discover elements 119 and 120. The excited nucleus has to shed this energy somehow. There are two ways to do this: by particle evaporation, or by fission. In particle evaporation, the nucleus will shed energy by releasing one or more neutrons (in this mass region), giving as a final product, say:

$$^{48}_{20}\mathrm{Ca} + ^{249}_{98}\mathrm{Cf} \rightarrow ^{297}_{118}\mathrm{Og}^{*} \rightarrow ^{294}_{118}\mathrm{Og} + 3\mathrm{n}. \tag{3}$$

This is shown schematically in Fig. 2(a). $^{294}_{118}$Og is your final product, which subsequently decays via α emission. In this case, you end up with very happy experimentalists. In total, five (perhaps 6) such decays have been observed. These reactions are very very very rare. 2.5×10^{19} ^{48}Ca atoms were used before the first decay of Og was seen. Far more frequently, fission will occur. In this case, the excited compound nucleus will split into two (rarely three) pieces of differing sizes, shown schematically in Fig. 2(b). The degree of competition between fusion-evaporation and fusion-fission depends on the excitation energy and angular momentum of the compound nucleus. However, **the presence of fission indicates the formation of a compound nucleus**. Thus, if you want to figure out the best way to form the next superheavy element, the best approach is to find a reaction that maximises the probability of capture – so you look at fission events. It's just not feasible to start out just looking for fusion-evaporation!

One thing that's common between the reactions producing elements 114 and 118 (and indeed, elements 113,115,116 and 117 too) is the use of ^{48}Ca as the projectile. That's because ^{48}Ca is especially useful for producing superheavy elements (for reasons we'll discuss later, and in the workshop). So in principle, to make a new superheavy element, you've just got to increase the number of protons in your target by one. The trouble is that the heaviest element you can sensibly make into a target is Californium (Cf), element number 98. We've run out of options to use a ^{48}Ca beam! This means that to get to element 119 and 120, we have to use a beam with more protons.

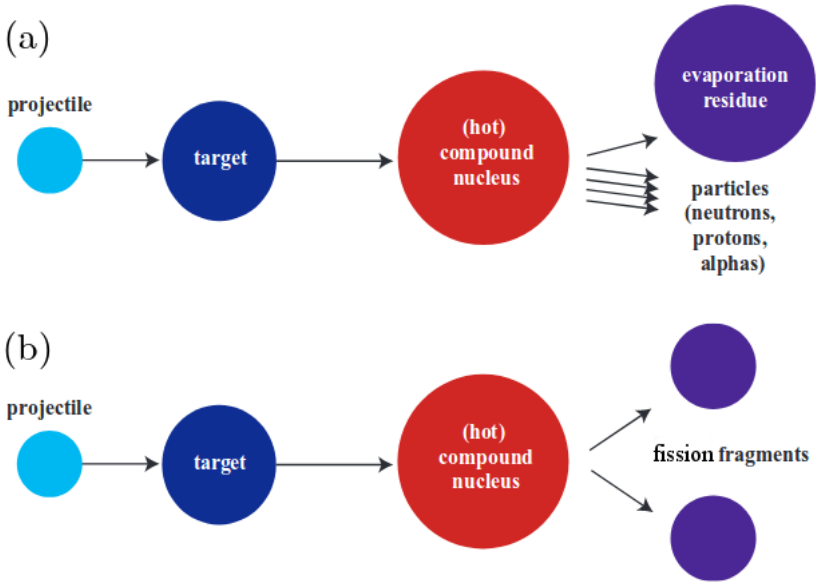

Figure 2: Schematic (not kinematically accurate) diagram of (a) fusion-evaporation and of (b) fission.

There's no shortage of elements with more protons than calcium, so what beam-target combination should we choose? The choice comes down to many factors, but an very important one is choosing a reaction that maximises your chance of forming that hot compound nucleus. This means that you need to make a choice that minimises a reaction outcome that we haven't talked about yet – quasifission.

4 Quasifission: Reactions competing with superheavy element creation

Quasifission, as the name suggests, is a reaction outcome that looks a bit like fission. Quasifission occurs when the colliding nuclei stick together for *not quite* long enough for a compound nucleus to form, and rotate a little bit (thanks to conservation of angular momentum) before separation. As the nuclei do stick around for a little while, there is a lot of mass transfer between the colliding fragments. It turns out that the amount of sticking time (and hence the number of rotations the nuclei undergo) is linked to the amount of mass transfer – very short sticking times correspond to very little mass transfer, and very long sticking times correspond to complete mass transfer, i.e. compound nucleus formation. The difference between fission and quasifission is shown schematically in Fig. 3.

Quasifission is one of the most important reactions competing with compound nucleus formation. It turns out, due to the structure and neutron-richness of ^{48}Ca, reactions with this projectile show less quasifission. Thus, to choose the reaction forming the next superheavy element, we have to figure out which reactions show mostly fission, and which show mostly quasifission. Since the amount of mass transfer and number of rotations is a signature of quasifission vs fission, we want to measure both the mass of the fragments and the angle at which they are flung out from the target.

The task of this workshop is the analysis of nuclear reaction data to first isolate events corresponding to fission and quasifission and to determine their masses and angles. This data was recently taken at the Australian National University, using the Heavy Ion Accelerator Facility. You can take a (work in progress!) virtual tour of the facility here: `http://people.physics.anu.edu.au/~ecs103/tour/`.

5 What you need to do before the workshop

- Have ROOT installed – the organisers will provide this to you.
- Read the appendix to the attached paper, found on page 13 of this pdf. This will give you an idea of how to use the measured velocity vectors for two fragments to determine their relative masses.

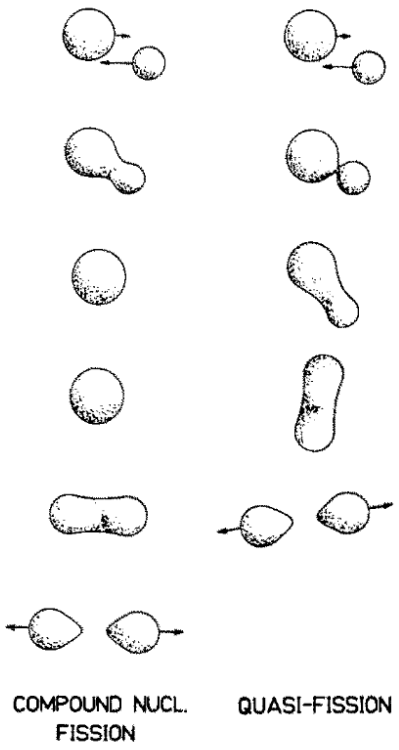

Figure 3: Sketch of fission following compound nucleus formation (left) and quasifission (right).

We've included the rest of the paper for completeness (and for the keen reader!) but you are not expected to have read it.

Conclusive evidence for the influence of nuclear orientation on quasifission

D. J. Hinde, M. Dasgupta, J. R. Leigh, J. C. Mein, C. R. Morton,* J. O. Newton, and H. Timmers
Department of Nuclear Physics, Research School of Physical Science and Engineering, Australian National University, Canberra, Australian Capital Territory 0200, Australia
(Received 10 November 1995)

Fission fragment anisotropies and mass distributions have been measured to high accuracy, over a wide range of angles, for the $^{16}O + ^{238}U$ reaction. The bombarding energies spanned the fusion barrier distribution, in steps of 1 MeV. Fission following transfer reactions was rejected by making use of the deduced velocity vectors of the fissioning nuclei. The resulting mass distributions for full momentum transfer fission show a small but significant skewness, which increases as the beam energy falls through the fusion barrier region, displaying a similar energy dependence as the fission fragment angular anisotropies. This is conclusive evidence for the interpretation that collisions with the tips of the deformed ^{238}U target nuclei lead to quasifission, while collisions with the sides result in fusion-fission.

PACS number(s): 25.70.Jj

I. INTRODUCTION

Measured fission fragment anisotropies for reactions of ^{12}C, ^{16}O, and ^{19}F projectiles on actinide targets [1–5] increase as the beam energy falls through the fusion barrier region. This is contrary to predictions based on the statistical transition state model of fission decay [6]. In this picture, fusion leads to a fully equilibrated compound nucleus, at its equilibrium deformation, which undergoes fission by passing over the true (unconditional) fission barrier. This is referred to subsequently as fusion-fission.

There are two classes of explanations for these anomalously large anisotropies. The first is that the parameters used in the transition state model (TSM) are wrong. Attention has been focused particularly on the mean-square angular momentum in fusion [1,4,5,7]. The second is that the transition state model itself is not applicable, because the fission fragments do not result from the decay of a fully equilibrated compound nucleus.

It was recently shown [8] that for the reaction $^{16}O + ^{208}Pb$, the transition state model, in conjunction with a standard barrier passing model of fusion, can describe the newly remeasured fission fragment anisotropies at energies both above and below the average fusion barrier. This result resolves a long-standing puzzle [1], and re-establishes confidence in TSM calculations of fission anisotropies at energies near the fusion barrier. It thus seems likely that the anomalously large anisotropies measured for actinide targets are evidence that at least some of the fission events do not result from the fusion-fission process.

It has been proposed that as well as fusion-fission, additional classes of fission exist. One, which has been called nonequilibrium fission [9], is proposed to occur following a fusion reaction and subsequent compound nucleus formation inside the true fission saddle point. In the case of a high fission probability, it was postulated [9] that fission may take place after equilibration of all degrees of freedom *except* the K degree of freedom. Here K is the projection of the total angular momentum on the nuclear symmetry axis; the mean square value of K at the fission saddle point determines the anisotropy. Nonequilibrium fission would have a large anisotropy. Models have recently been described which attempt to explain the large sub-barrier fission anisotropies in the framework of the nonequilibrium fission picture. One is for fission where the mass asymmetry in the entrance channel is less than the Businaro-Gallone critical asymmetry [10], while one is applicable specifically to reactions on deformed actinides [11].

Another type of fission has been termed quasifission [12,13]. This is conceptually quite distinct from nonequilibrium fission, in that the fusion process is not followed by compound nucleus formation inside the fission saddle point. Instead, the configuration of the dinucleus, initially trapped inside the conditional saddle point, evolves over the potential energy surface and crosses the saddle line before reaching mass symmetry, as experimental results demonstrate [13]. Thus in principle there is always some memory of the mass and direction of the projectile in the initial collision. This should result in a measurable correlation of fragment mass with angle, unless the system lives long enough to rotate many times. Such a correlation cannot exist if the system passes from the equilibrium configuration over the true fission saddle point. The quasifission anisotropies are large, because the dinucleus never becomes compact, and additionally, K equilibration may not be attained.

To distinguish unambiguously between the two possible explanations described above requires the measurement of fission mass distributions at forward or backward angles, to determine whether there is a correlation of mass with angle. Such a measurement was made [1] for the reaction $^{12}C + ^{236}U$, where a small anomaly in the anisotropies was observed, but it was concluded that there was no evidence for quasifission. Either the effect was too small to be identifiable in that measurement, or quasifission is not responsible for the large anisotropies.

It has been shown [3] that the characteristic energy dependence of the measured fission anisotropies for the reaction $^{16}O + ^{238}U$ is consistent with a picture where collisions with

*Present address: Department of Physics, State University of New York at Stony Brook, Stony Brook, New York 11794.

the tips of the deformed ^{238}U target nuclei lead to quasifission, while collisions with the sides result in fusion-fission.

This paper reports on a complete analysis of these data, with particular emphasis on a detailed investigation of the fission fragment mass distributions, to search for evidence of quasifission in the mass spectra.

II. EXPERIMENTAL PROCEDURE

The experiment was carried out using pulsed beams of ^{16}O, from the 14UD tandem electrostatic accelerator at the Australian National University, over an energy range 76 MeV $\leqslant E_{\rm lab} \leqslant$ 112 MeV. The pulse width was $\simeq$ 1.5 ns, with a pulse separation of 106.6 ns. The target of UF_4 was $\simeq$220 μg cm^{-2} in thickness, on a $\simeq$15 μg cm^{-2} C backing. The backing faced downstream, so as not to degrade the beam energy before interaction with the ^{238}U. To allow calibration of the mass distributions, measurements were also made with a C-backed $\simeq$24 μg cm^{-2} target of ^{208}PbS. Fission fragments were detected in large area multiwire proportional counters (MWPC's), position sensitive in two dimensions. Each had an active width of 284 mm, and height 357 mm. The time signals from the position-sensing wires, separated by 1 mm, passed through delay lines with 1 ns delay between each wire. Position resolution was $\approx$ 1 mm. The detectors were placed 180 mm from the target, giving a scattering angle coverage of $95° \leqslant \theta_{\rm lab} \leqslant 170°$ in the backward hemisphere, and $10° \leqslant \theta_{\rm lab} \leqslant 85°$ in the forward hemisphere. Signals in the forward detector were only accepted when in coincidence with the backward detector. The central foils of the MWPC's provided energy loss and arrival time signals. The position information allowed these signals to be corrected for the significant geometrical effects caused by the large angular acceptance of the detector, permitting precise determination of particle velocities. Each event at position (x,y) on the active area of the detectors was transformed to give the scattering angle $\theta_{\rm lab}$ with respect to the beam axis, and the azimuthal angle $\phi_{\rm lab}$. The differential cross sections $d\sigma_{\rm fis}/d\Omega$ were obtained by calibrating each 5° bin with Rutherford scattering at a far sub-barrier energy. Details of this procedure are described in Ref. [8]. Two Si surface-barrier detectors, positioned in the vertical plane at $\pm 22°$ relative to the beam axis, were used to count the elastically scattered yield, providing a normalization between the calibration and the fission measurements.

III. EXPERIMENTAL ANALYSIS AND RESULTS

The measured fission yield for reactions on actinide targets contains three components. The first results from fission of the targetlike nuclei, which occurs by excitation over the fission barrier during transfer reactions, in grazing collisions. The second component, which is of interest here, results from fission following complete amalgamation of the projectile and target, in more central collisions. This is referred to subsequently as full momentum transfer (FMT) fission. The third component results from fusion following break-up of the projectile, which is referred to as incomplete fusion. Its presence is revealed by an asymmetry in the folding angle distribution. It occurs at bombarding energies well above the fusion barrier, and is not expected to be significant at the energies of interest here, nor is there any evidence for it in these experimental data.

The first requirement in the analysis is separation of the transfer fission from the FMT fission. The result of a preliminary analysis of these measurements was given in Ref. [3]. In that work, transfer fission was separated from FMT fission using the measured fission fragment folding angles. A more complete data analysis, making use of the fission fragment velocities is described below. This results in better separation of the two components, and in addition allows extraction of the fission fragment mass distributions.

A. Rejection of transfer fission

A new method was developed to cleanly separate the transfer fission from the FMT fission, event by event. This was achieved through the experimental determination of *two* components of the velocity vector of each fissioning nucleus. The component in the beam direction, denoted by $v_{\rm par}$, was deduced from the folding angle and the velocities of the two fragments. The other component $v_{\rm perp}$ is in the plane perpendicular to the beam, and is perpendicular to the projection of the scission axis onto this plane. It was determined from the azimuthal folding angle and the projection of the measured fragment velocities onto this plane. Details are given in the Appendix.

Figure 1 shows scatter plots of the measured $v_{\rm par}$ against $v_{\rm perp}$, for an angular range of $\theta_{\rm lab} = 95°$ to 105°. Panels (a) and (b) correspond to beam energies below and well above the average fusion barrier, respectively. For FMT fission, the distribution of $v_{\rm perp}$ would be expected to be centered around zero, while at the low beam energies of interest here, $v_{\rm par}$ would be expected to peak around the center-of-mass velocity $v_{\rm c.m.}$. The high intensity regions in the middle of the plots thus correspond to FMT fission. For fission following a transfer reaction, $v_{\rm perp}$ would be expected to be close to zero only in the case that the fission occurs in the plane of the transfer reaction, otherwise $v_{\rm perp}$ is only constrained by kinematical limits, which will generally force transfer fission events to lie inside a circle of radius $v_{\rm c.m.}$, centered at $v_{\rm par}=v_{\rm c.m.}$, $v_{\rm perp} = 0$. At energies below the fusion barrier, where the projectilelike nucleus recoils to backward angles, $v_{\rm par}$ for transfer fission events will be larger than $v_{\rm c.m.}$, while at energies well above the fusion barrier, where the projectilelike nucleus continues to forward angles, $v_{\rm par}$ will be smaller than $v_{\rm c.m.}$. The scatter plots indeed show events corresponding exactly to these expectations, lying within the circles of radius $v_{\rm c.m.}$. It is noteworthy that a large fraction of transfer fission events do occur out of the plane of the transfer reaction. This feature, though interesting, is not the subject of this paper, and will not be further discussed here.

Light particles (n,p,α particles) will be evaporated from the nuclei before scission, or from the fission fragments. This results in a slight broadening of the distribution of velocity components expected from the kinematics of the massive reaction products alone, and also gives a small spread to the observed correlation angles. It can easily be shown that at center-of-mass angles $\theta_{\rm c.m.}$ around 90°, this spread in angle results in a slight spreading in both the deduced $\theta_{\rm c.m.}$ and mass; this is however small compared to the characteristic angular and mass variation intrinsic to the fission process. At

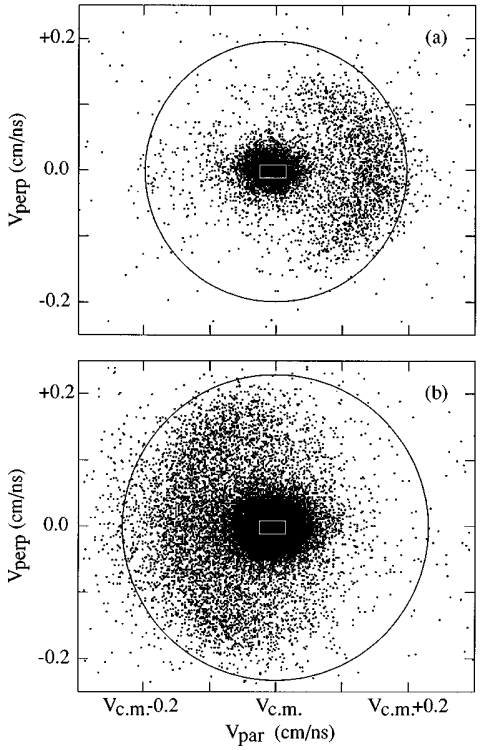

FIG. 1. Experimentally determined velocity components of the fissioning nuclei $v_{\rm par}$ and $v_{\rm perp}$, for beam energies below (82 MeV) and well above (112 MeV) the average fusion barrier for ^{16}O + ^{238}U, shown in panels (a) and (b), respectively. $v_{\rm par}$ is plotted relative to the calculated center-of-mass velocity $v_{\rm c.m.}$ for each energy. FMT fission events lie in the center of the figures, while transfer fission events are spread out within the circles of radius $v_{\rm c.m.}$, as expected. The white rectangles indicate the cut used to select the FMT fission events for the mass-spectrum determination.

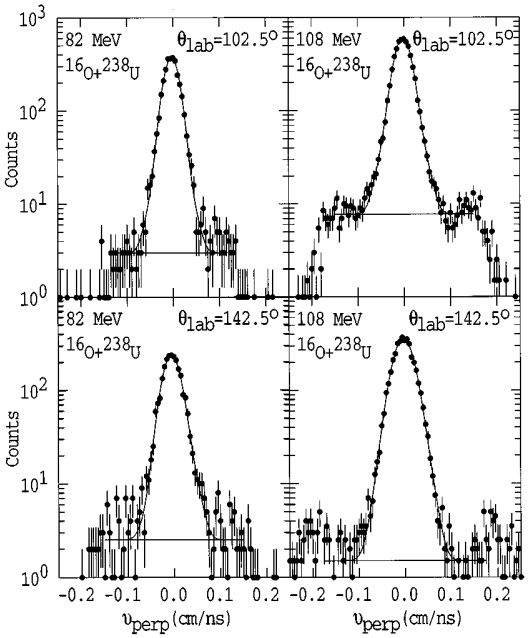

FIG. 2. Projections of the deduced quantity $v_{\rm perp}$ (see text) for low and high beam energies (left and right sides, respectively) at the two representative laboratory angles indicated. Each spectrum includes an angular range of 5°. Fission events beyond the central peak correspond to transfer fission. The transfer fission yields subtracted from the central (FMT) region are indicated by the horizontal lines.

angles close to the beam direction, the different geometry leads to a significant spread in both $v_{\rm par}$ and mass. However, if in the determination of the masses, the experimentally determined value of $v_{\rm par}$ is not used, but rather $v_{\rm par}$ is fixed to be equal to $v_{\rm c.m.}$, then only the small effect of the spread in velocities remains, and accurate mass spectra can also be obtained at these angles. At such angles, the deduced values of $v_{\rm par}$ are spread beyond the kinematical limits discussed above, but the separation of FMT fission from transfer fission is not compromised.

The assumption that $v_{\rm par}=v_{\rm c.m.}$, which is made in the mass determination, is reasonable for the FMT fission events, because the bombarding energies involved are low, leading to the expectation that the incomplete fusion yield should be negligible. Experimental evidence supporting this expectation comes from the observation, at angles where the deduced $v_{\rm par}$ is reliable, that the deduced $v_{\rm par}$ spectra show a single symmetric peak. The assumption is not appropriate to determine mass spectra for the transfer fission events, but since one objective of the analysis is to reject such events, it causes no problem.

To deduce the yield of fission following full momentum transfer, a cut on $v_{\rm par}$ was applied which varied with $\theta_{\rm c.m.}$. This cut accepted 99% of FMT fission events, but removed a substantial fraction of transfer fission events, as would be expected from inspection of Fig. 1. The resulting spectra of $v_{\rm perp}$ were projected, typical examples being shown in Fig. 2. The transfer fission component under the FMT peak was estimated and subtracted by performing a linear fit to the transfer fission yield adjacent to the FMT peak, as illustrated. The background varied with energy and angle, but was at most a few percent of the FMT yield.

From these data the FMT fission angular distributions were determined, and were fitted by varying the parameters of the transition state model describing angular distributions for fission following fusion [12]. This fit procedure resulted in reasonably good representations of the experimental data, and allowed the fission anisotropies to be determined from the ratio of the extrapolated yields at $\theta_{\rm c.m.}=90°$ and 180°. The total fission cross sections were also obtained from the fits. It is possible that a systematic error may be introduced by using angular distributions calculated within the TSM to extrapolate to $\theta_{\rm c.m.}=90°$ and 180°, however since the experimental data spanned an angular range $110°\leqslant\theta_{\rm c.m.}\leqslant160°$, this could only cause a small change in the anisotropies, and a negligible change in the cross sections.

The error bars shown in Fig. 3 correspond only to statistical uncertainties, which were determined from the χ^2 envelopes obtained in fitting the angular distributions. The high statistics obtained at each energy (at $E_{\rm c.m.}$ around 75 MeV, $\sim10^4$ fission events were measured, increasing to $\geqslant10^5$ at $E_{\rm c.m.}\geqslant85$ MeV) result in low statistical uncertainties. The observed scatter of the points suggests that there are no significant additional sources of random uncertainties.

It should be noted that the method of rejecting transfer fission based on determination of $v_{\rm par}$ and $v_{\rm perp}$ does not

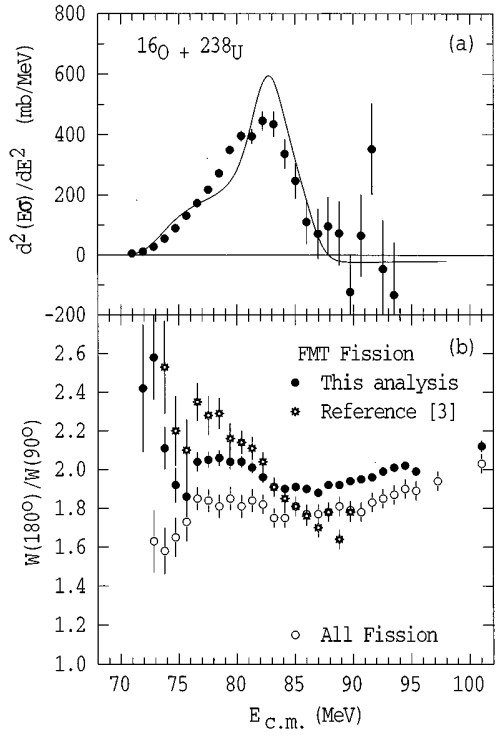

FIG. 3. Panel (a) shows for the $^{16}O + ^{238}U$ reaction the second derivative with respect to energy of the fusion excitation function multiplied by $E_{\text{c.m.}}$, which is proportional to the fusion barrier distribution. The calculation is described in the text. The fission anisotropies for the $^{16}O + ^{238}U$ reaction are shown in panel (b). Hollow points represent the case where no discrimination against transfer fission is made. The solid points represent the anisotropies for FMT fission only, when selected using the velocity components of the fissioning nuclei, as described in the text. The stars show the anisotropies for FMT fission when using the folding angle to discriminate against transfer fission.

require the fission fragment velocities to be known to very high accuracy, since the FMT fission events can be easily identified and separated from the transfer fission events. The mass-spectrum determination, described in Sec. III D, does however require a very accurate velocity determination.

B. Fusion barrier distribution

The fusion process in the $^{16}O + ^{238}U$ reaction is expected to be strongly influenced by the static deformation of ^{238}U. For this reaction, the fusion cross sections σ_{fus} can be identified with the measured FMT fission cross sections, due to the very small survival probability of evaporation residues [14]. The fusion barrier distribution [15] was determined from the second derivative of the function $E_{\text{c.m.}}\sigma_{\text{fus}}$ with respect to $E_{\text{c.m.}}$, using a point-difference formula [16] with an energy step of 1.87 MeV. It was shown experimentally [16,17] for the reaction $^{16}O + ^{154}Sm$ that a deformed nucleus with a prolate deformation and a positive hexadecapole deformation displays a very distinctive fusion barrier distribution, which is characteristic of its static deformation. The nucleus ^{238}U has similar deformation parameters to ^{154}Sm, and the shape of the measured fusion barrier distribution proves to be very similar. This distribution is shown in Fig. 3(a). The shape is almost identical to that determined from the FMT fission yields which were obtained in the earlier folding angle analysis of the data [3].

The fusion barrier distribution resulting from a geometrical calculation, using the code CCMOD [18], with tabulated [19] quadrupole and hexadecapole deformation parameters, is indicated by the solid line. Coupling to the 3^- state in ^{238}U is included. The calculation represents well the main features of the measured distribution. The small discrepancies can be reduced by the inclusion of other weak couplings in the calculation. These will be discussed elsewhere. The fact that some of the fission yield results from quasifission does not invalidate the comparison of measurement and theory. This point is extensively discussed in Ref. [20].

It is concluded that the deformation of ^{238}U plays a dominant role in the fusion process, and to a good approximation it can be modeled classically as a static deformation. This conclusion is vital for the subsequent interpretation of the fission anisotropies and mass distribution data.

C. Fission fragment anisotropies

The deduced fission anisotropies $W(180°)/W(90°)$ are shown in Fig. 3(b), for the case where no discrimination against transfer fission is applied (outlined circles), and where only FMT fission is selected as described above (solid circles). The anisotropies extracted for FMT fission from the folding angle analysis of Ref. [3] are shown by stars. The current FMT anisotropies are quantitatively somewhat different from the former, due to the better separation of transfer fission from FMT fission in the present analysis. Nevertheless, qualitatively they show the same feature as was presented in that work (and in another measurement for this reaction [2] also based on the folding-angle technique), namely, a significant rise in the anisotropy as the beam energy falls through the fusion barrier region. This is in contrast to TSM predictions of a decreasing anisotropy.

D. Determination of fission mass distributions

To test for the presence of quasifission, it is sufficient to measure mass ratios (the ratio of the observed fragment mass at scission to the total mass at scission), which will be denoted by M. Since only small deviations from a completely symmetric mass distribution are expected, extreme care was taken to obtain accurate mass spectra, free of systematic errors, as detailed below.

Fission fragment mass-ratio spectra can be determined from the angle and time-of-flight information obtained in the experiment, based on the principle of conservation of linear momentum, as described in the Appendix. The two fission fragment velocities must be determined very accurately, which requires calibration of each of the two fission fragment time-of-flight spectra, knowledge of the flight path for each event, and accurate determination of the time zeros of each time-of-flight spectrum. The last is the most difficult to determine. A technique making use of a calibration reaction was employed to determine the time zeros for each beam energy. This involved making measurements for the $^{16}O + ^{208}Pb$ reaction, which were interleaved with the $^{16}O + ^{238}U$ measurements at both low and high beam energies. By assuming that the fission mass spectrum from the calibration

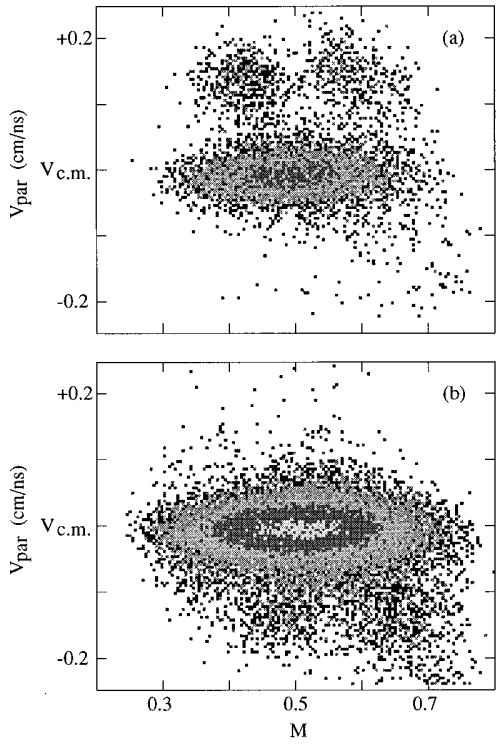

FIG. 4. Scatter plot of deduced mass-ratio M against the parallel velocity component of the fissioning nuclei v_{par}, for the same beam energies as in Fig. 1. FMT fission events lie in the center of the figures, while transfer fission events, with an asymmetric mass distribution, lie at higher and lower v_{par} values, respectively.

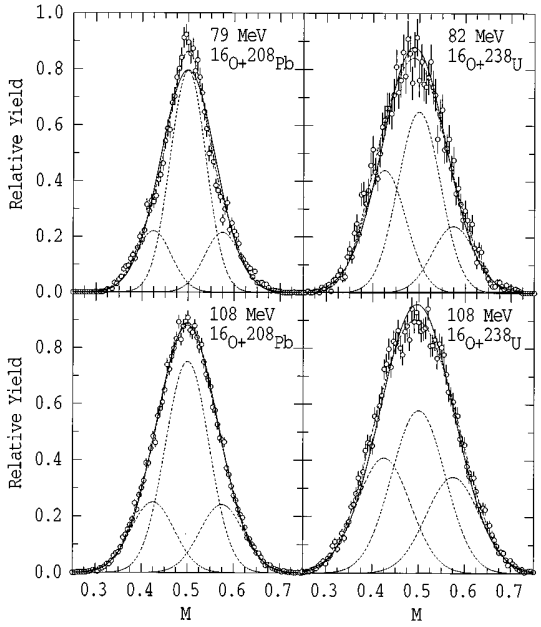

FIG. 5. Representative mass distributions for the two reactions, integrated over the angular range $110° \leqslant \theta_{\mathrm{c.m.}} \leqslant 155°$, shown in terms of the ratio of the fragment mass in the back angle detector to the summed masses of the two fragments. This is denoted by M. The indicated beam energies are below (upper panels) and well above (lower panels) the average fusion barriers for each reaction. Fits by a single Gaussian, and by three Gaussians, are shown by the solid and dashed lines, respectively.

reaction is symmetric (and making a very slight correction due to energy loss in the target, resulting in an expected value of the mass ratio in the back angle detector of $M=0.499$), the difference in time zeros for the two time-of-flight spectra was determined. This difference was constant to $\pm$ 25 ps over a number of energies. The high energy data were used, because of the good statistics. The absolute time zeros for each reaction and energy were determined by requiring that the average value of v_{par} should equal the calculated $v_{\mathrm{c.m.}}$, taking into account the small corrections due to energy loss in the target. Thus reliable mass-ratio distributions were extracted at each bombarding energy. The position of the centroids of the distributions proved to be sensitive principally to the difference between the time zeros, and relatively insensitive to changes in the assumed value of v_{par}.

Figure 4 shows scatter plots of the mass ratio M for the back detector as a function of v_{par}. The reactions and angular range are the same as for Fig. 1, but a cut on v_{perp} of $\pm$ 0.05 cm/ns was applied, to reduce the transfer fission component. These plots illustrate the apparently symmetric FMT fission, with v_{par} centered around $v_{\mathrm{c.m.}}$, and show that despite assuming the kinematics for FMT fission, the mass distributions for transfer induced fission display a clear double-peaked structure, as would be expected.

For the ^{16}O + ^{208}Pb reaction, no further data processing was necessary, however for the ^{16}O + ^{238}U reaction, further measures were taken to minimize the contribution from transfer fission. A narrow cut around the peak in v_{par} (corresponding to $\pm$ 0.02 cm/ns) was applied, in addition to a narrower cut on v_{perp} of $\pm$ 0.01 cm/ns. These restrictions, indicated on Fig. 1 by the white rectangles, reduced the estimated transfer fission contamination to a small fraction of 1%. The data for all center-of-mass angles between 110° and 155° were summed to maximize statistical precision. These angular limits were chosen to ensure that no cut was applied to the mass spectra due to the angular acceptance limits of the detectors. These velocity and angular cuts were in fact also applied to the ^{16}O + ^{208}Pb data. This avoids the possibility of introducing small systematic errors, although for this reaction the difference between the mass spectra with and without these cuts was negligible.

Any deviation from symmetry in the mass ratio spectra, whose average angle is $\sim$ 135°, can be attributed to a correlation of fission mass split with angle, due to the presence of quasifission.

Typical mass ratio spectra for energies below and above the respective fusion barriers are shown in Fig. 5, both for the ^{16}O + ^{208}Pb reaction (left panels) and the ^{16}O + ^{238}U reaction (right panels). It is important to note that no assumption was made regarding the mass distribution for the low energy ^{16}O + ^{208}Pb data. They were treated in exactly the same way as the ^{16}O + ^{238}U data, and the degree to which they show the expected symmetric mass distributions represents an excellent control measurement, and indicates the reliability of the calibration methods used, and thus of the mass spectra extracted for the ^{16}O + ^{238}U reaction.

E. Characterization of fission mass distributions

The fission mass distributions were initially fitted by a single Gaussian. The high energy ^{16}O + ^{208}Pb data were

well reproduced, however, there were significant discrepancies between the data and the fits, both for the $^{16}O + ^{238}U$ data, and, perhaps surprisingly, for the low energy $^{16}O + ^{208}Pb$ data. This is shown in Fig. 5, where the single Gaussian fits are indicated by full lines.

The deviations between the fits and the $^{16}O + ^{238}U$ data are particularly apparent for $M \sim 0.4$. This deviation is consistently present, and demonstrates that there is a small but definite skewness in the mass distributions. The low energy $^{16}O + ^{208}Pb$ data exhibit no such skewness, but do show a narrow central peak and slight shoulders in the mass distributions, which are not well reproduced by a single Gaussian. These characteristics may be attributed to components of mass symmetric and mass-asymmetric fission, the latter probably being associated with last-chance fission. Recent results [21] confirm the presence of this asymmetric component in the mass distribution at low beam energies.

To investigate the energy dependence of the mass spectra, the moments of the M distributions were evaluated, and the values of the variance (σ_M^2) and mean ($\bar{M}$) were determined. They are shown in Figs. 6(a) and (b), respectively. The variance falls smoothly with decreasing energy in both reactions, giving little insight into the detailed variation with energy of the mass spectrum. The mean mass split for $^{16}O + ^{208}Pb$, as expected, is centered at 0.499 (see Sec. III D) for both high and low energies, indicating no correlation of mass with angle. For the $^{16}O + ^{238}U$ reaction, $\bar{M}$ is not centered at 0.500, but is slightly below at the higher energies, averaging $\bar{M} \simeq 0.497$, and makes a transition at $E_{\text{c.m.}}$ around 83 MeV to a value of $\simeq 0.490$. This is a small effect, however having the $^{16}O + ^{208}Pb$ data as a control makes its significance convincing.

The fact that the centroids of the mass distributions for the $^{16}O + ^{238}U$ reaction are below $\bar{M} = 0.500$ cannot be attributed to energy loss in the target, and is by itself good evidence for the validity of the quasifission interpretation of the large fission angular anisotropies. However, as will be shown, the energy dependence of $\bar{M}$ provides even better evidence.

The skewness of each M distribution was also evaluated, from the second and third moments of the distribution. The values showed a relatively large scatter, which was attributed to sensitivity to fluctuations in the yield at the extremes of the mass distributions.

Instead of pursuing further the moments of the mass distributions, a method of characterising the data was chosen which is more transparent, and may be more closely related to real physical processes occurring. It was found that all the $^{16}O + ^{238}U$ mass distributions could be fitted well by the sum of three Gaussians with fixed positions. The lowest χ^2 values were obtained if the Gaussians were centered at $M =$ 0.425, 0.500, and 0.575. The widths of the three Gaussians were constrained to be equal, but the common width was varied, along with the three intensities, to give the optimum fit to each mass spectrum. The components and the fits are indicated by the dashed lines in Fig. 5.

Both the centroid shift and the skewness will significantly affect the ratio of the intensities of the two outer Gaussians, thus the deviation of the mass distribution from a symmetric shape can be characterized by this ratio, denoted by G_1/G_3. These data are shown in Fig. 6(c), for both reactions. The FMT angular anisotropy data for $^{16}O + ^{238}U$ are shown in Fig. 6(d).

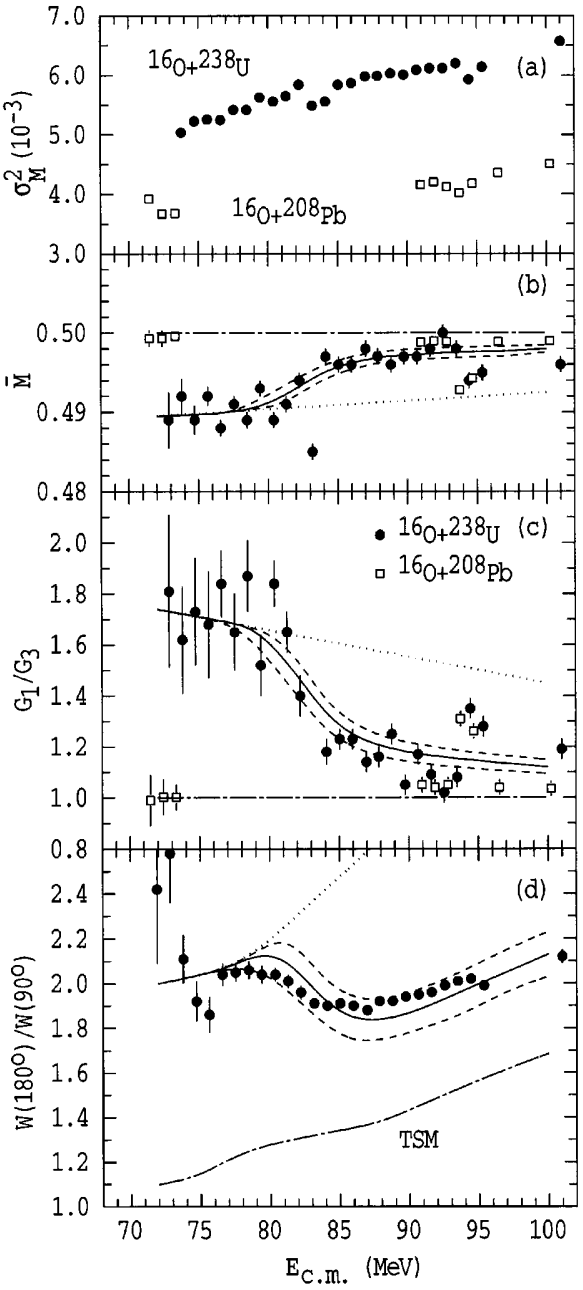

FIG. 6. Panel (a) shows the energy dependence of the variance of the M distribution, for the two reactions. Panel (b) shows the mean values of M, while panel (c) shows the ratio of the yields of the lower and upper of the three Gaussians fitted to the fission mass distributions. Panel (d) shows the fission angular anisotropy. All data correspond to FMT fission only. The expectations based on the transition state model are shown by the dot-dashed lines. The assumed behavior for quasifission is shown by the dotted lines. The calculations which reproduce the energy dependence of the data (solid lines) are described in the text.

A number of features of the data will be commented on, before proceeding further with the interpretation.

(i) For both reactions, at $E_{\text{c.m.}} \simeq 94$ and 95 MeV, most of the measured quantities show anomalous values. This is at-

tributed to a transient problem in the electronics for these energies; these data were not used in the calibration.

(ii) The excitation function was measured by increasing the beam energy during the course of the experiment. To test for the possible presence of systematic errors introduced by this procedure, the point at $E_{\text{c.m.}} = 76.8$ MeV was measured at the end of the run. It shows no discrepancy compared to neighboring points measured at the beginning of the run, which is good evidence for the absence of such errors.

(iii) As well as the three-Gaussian fit, two Gaussians were fitted to the mass spectra. Although the ^{16}O + ^{208}Pb data could not be well reproduced, the energy dependence of the ratio of the yields for the ^{16}O + ^{238}U data was the same as that of G_1/G_3, showing that the energy dependence observed was not an artefact of the three-Gaussian fit.

F. Transition state model predictions

The predictions of the measured quantities for the case of fusion-fission are made with the transition state model (TSM). It is implicit in the TSM that the mass distributions will be symmetric at all angles, independent of beam energy. Thus $\bar{M}$ is expected to be 0.500 and G_1/G_3 to be 1.0. These values are indicated by the dot-dashed lines in Fig. 6(b) and 6(c). The fission angular anisotropies were calculated as described in Ref. [8], using the exact expressions of Ref. [12]. The dependence of the calculated anisotropy on the input parameters can be easily seen from the approximate expression for the anisotropy

$$W(180°)/W(90°) \approx 1 + \frac{\langle J^2 \rangle \hbar^2}{4(T \mathscr{J}_{\text{eff}})}, \tag{1}$$

where $\mathscr{J}_{\text{eff}}$ is the effective moment of inertia of the saddle-point (transition state) configuration and T is the temperature at the saddle point. J is the angular momentum at the saddle point, which is closely related to the orbital angular momentum in the fusion reaction. The effective moment of inertia, as a function of angular momentum, was taken from a simple parametrization [22] of the rotating finite range model. This gives larger effective moments of inertia than are obtained from the liquid drop model, and thus results in smaller calculated anisotropies than those in Ref. [12]. The fusion angular momentum distributions were taken from a CCMOD calculation which best fitted the fusion excitation function. The deduced FMT fission cross sections are smaller than those in Ref. [12], perhaps due to the better rejection of transfer fission, thus the deduced angular momentum distributions do not extend as high in J. This difference also results in a reduction of the calculated anisotropies. The combination of these two effects causes the calculated fission anisotropies, indicated by the dot-dashed line in Fig. 6(d), to remain well below the data, even at the higher beam energies. This is in contrast with the reasonably good agreement found in Ref. [12]. In the calculation shown, it was assumed that the presaddle fission delay time is zero [20]. The use of a presaddle delay time adjusted to reproduce prescission neutron multiplicities for a similar reaction [23] increases the TSM anisotropies only slightly at bombarding energies in the barrier region, as was also found in Ref. [20].

The results in Fig. 6 show that the measured quantities deviate substantially from the TSM expectations at the low energies, but approach closer to them as the energy increases through the fusion barrier region. This suggests that the same physical effect is responsible in each case for the deviation from the TSM calculations.

IV. DISCUSSION

Considering the collision classically, the highest energy fusion barriers correspond to contact of the projectile with the flattened side of the prolate target, resulting initially in a compact dinuclear system. Conversely, the lowest energy fusion barriers correspond to contact with the tip, giving an elongated dinuclear system. Intuitively, it seems reasonable that the former configuration would be more likely to result in fusion-fission, and the latter in quasifission.

A. Simple geometrical model

A simple empirical geometrical model to test this picture was proposed in Ref. [3]. It was assumed that collisions with the tips of the target nuclei result in quasifission only; the data at the lowest energies then define the values of $\bar{M}$, G_1/G_3, and $W(180°)/W(90°)$ for quasifission at these energies. The energy dependence assumed is shown by the dotted lines in Fig. 6. For the mass spectra, increased rotational frequency with increasing beam energy may be expected to attenuate the observed asymmetry, thus a linear trend toward symmetry was assumed, as shown in Figs. 6(b) and 6(c). Taking energy-independent values of $\bar{M}$ and G_1/G_3 for quasifission does not however change the results appreciably.

The assumption of an increasing angular anisotropy with beam energy for quasifission [shown in Fig. 6(d) by the dotted line] is reasonable, based on the observation of rapidly increasing anisotropies for reactions where quasifission is dominant [12,20].

A sharp transition between quasifission and fusion-fission was assumed to occur at a critical fusion barrier radius. The average values of $\bar{M}$, G_1/G_3, and $W(180°)/W(90°)$ were determined at a given beam energy using the values assumed for quasifission, and the values for fusion-fission based on the TSM. Each was weighted by the corresponding cross sections resulting from passage over fusion barriers with radii, respectively, greater and smaller than the critical radius. At low beam energies, only contact with the tips of the target nuclei are possible, resulting in quasifission. Above the fusion barrier region, all orientations of the target nuclei result in contact, leading to a mix of quasifission and fusion-fission events, and to average values of measured quantities which lie between those for quasifission and those for fusion-fission.

Taking a critical radius corresponding to an angle between the beam axis and the target nucleus symmetry axis of 35°, the resulting predictions are indicated by the solid curves in Figs. 6(b), 6(c), and 6(d). The calculations follow the trends of the data very well. In reality, a sudden transition at 35° is not likely, due to fluctuations in the trajectories. The effects of a $\pm 5°$ change in angle are indicated by the dashed lines; it is evident that a smooth transition may agree even better with the data. The success of these simple calculations strongly supports the hypothesis that collisions with the tips

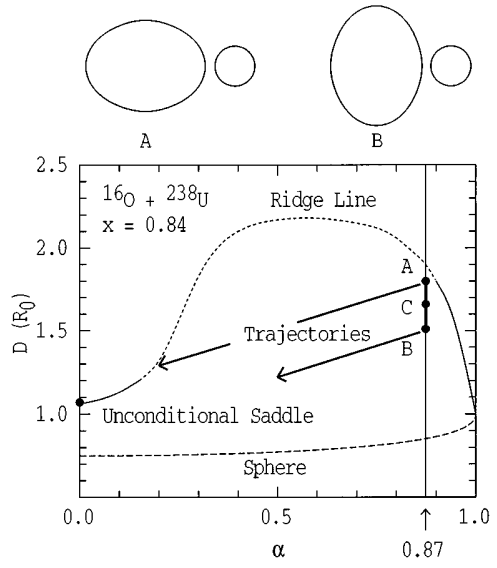

FIG. 7. The fusion barrier configurations for $^{16}O+^{238}U$ corresponding to collision with the tips (A) and sides (B) of the deformed ^{238}U. These points are indicated on the potential energy surface, as a function of the center-of-mass separation D and the mass asymmetry α. The spherical configuration and the estimated position of the conditional fission saddle ridge line are shown. Possible trajectories are sketched from injection points A and B, leading to quasifission and fusion-fission, respectively.

of the deformed target nuclei result in quasifission, while collisions with the sides result in fusion, followed by complete equilibration, and statistical decay resulting almost always in fission.

B. Orientation dependence of quasifission

A number of possible explanations can be put forward as to why collisions with the tips of the deformed target nuclei result in quasifission, while collisions with the sides result in fusion. They are discussed below.

One likely scenario for such shape dependence of the competition between fusion-fission and quasifission was discussed in Ref. [3]. Once inside the fusion barrier, the radial motion is rapidly damped, and the nuclear system will start to evolve in shape over the potential energy surface (PES). Important features of the PES for this system are sketched in Fig. 7. The abscissa represent the mass-asymmetry α, defined in terms of the masses (or mass ratios) of the heavy and light fragments: $\alpha=(M_H-M_L)/(M_H+M_L)$. The ordinate represents the separation D of the centers of mass of the two incipient fragments, defined in units of the radius of the spherical configuration (R_0), as in Ref. [24]. The equilibrium configuration, which should be reached for fusion-fission to occur, is close to the dashed line corresponding to a sphere. The ridge line represents the locus of configurations of the conditional (α fixed) saddle points. If D is outside the ridge line, the PES forces the system to scission. The curve in Fig. 7 was estimated by extrapolation from the results of Ref. [24] for lighter nuclei, since for fissile systems such as this, it proved possible to define the ridge line only at large and small α (solid line). At intermediate values of α the larger fragment may be thought of as deformed outside its own saddle point [24]. Nature must provide an effective ridge line, since even the quasifission mass spectra are nearly symmetric, however its location should be at smaller values of D than indicated by the dashed line.

The trajectories over the PES will depend in detail on the features of the PES and the inertia and viscosity tensors. Experimental evidence [13] shows that the mass-asymmetry degree of freedom equilibrates more rapidly than does the elongation. Thus qualitatively, the trajectory leading from the most compact injection point (B) may be as indicated on Fig. 7 by the arrow, resulting in fusion-fission. Moving the injection point out to the largest value of D, corresponding to the largest fusion radius, at point A in the figure, should cause the system to cross the ridge line at finite asymmetry as illustrated, resulting in quasifission. The experimental data presented in this work indicate that the transition between quasifission and fusion-fission occurs around point C. The combined effect of the larger effective moment of inertia compared to that of the unconditional saddle point at $\alpha=0.0$, and the fact that K equilibration [9] may not be achieved, will result in a large anisotropy.

The critical parameter in this picture is the difference between the elongation of the unconditional saddle point, and the elongation of the fusion configuration. Where this difference is large, quasifission results, while where it is small, fusion-fission results.

This description assumes that after the projectile and target nuclei join together, the average trajectory results in the projectilelike part of the dinucleus gaining mass at the expense of the targetlike part, as the dinucleus evolves in shape. Whether the system evolves in this direction, toward $\alpha=0.0$ or toward $\alpha=1.0$, is expected to be determined by the PES. In particular, the Businaro-Gallone critical asymmetry α_{BG} [25] defines the point on the ridge line where the potential energy is at its maximum. It separates the region of smaller asymmetries (more symmetric projectile and target masses), where the projectile ''sucks'' mass from the target, and the region of larger asymmetries where the reverse happens. For this system, α_{BG} can be estimated by extrapolation of the results of Ref. [24] to be $\sim$ 0.90, while the injection point is at $\alpha=0.87$ (before N/Z equilibration). Thus the projectilelike partner should gain mass, and the system should move towards mass symmetry.

The calculations [24] of the conditional saddle points were made allowing all the shape degrees of freedom to vary, subject to the constraint that α was fixed. This does not necessarily correspond to the situation during the early stages of equilibration following fusion. The present experimental results indicate that the targetlike component of the dinucleus retains some memory of its initial deformation, and orientation. The change in Coulomb energy resulting from charge transfer will depend on whether the projectilelike component is ''stuck'' to the side or to the tip of the targetlike component. It would be interesting to have theoretical calculations for a fixed targetlike shape corresponding roughly to the ^{238}U ground-state deformation, which could show whether α_{BG} shifts in asymmetry, depending on the relative orientation of the symmetry axis of the targetlike component of the dinucleus, and the axis joining the centers of the two components. The change in the Coulomb energy resulting from charge transfer will certainly depend on the

relative orientation, so it is not unlikely that the peak position may shift.

If the peak shift were in the appropriate direction (consideration of the Coulomb energy change alone would indicate that it is), a second explanation for the observed shape dependence of the quasifission and fusion-fission competition becomes possible. In this picture, collisions with the tips of the target nuclei would result in movement toward mass symmetry, and may lead to quasifission, while collisions with the sides would result in absorption of the projectile by the target, and thus to the standard fusion-fission process. The theoretical calculations however need to be carried out to see whether this possible explanation needs to be taken seriously.

The current experimental data alone cannot distinguish which one, if only one, of these possible qualitative explanations is closest to the true situation. Clearly, it is only by modeling the dynamical processes occurring during the collision, and successfully describing the experimental data, that a full understanding of the physical situation can be developed. It may well be that trajectory fluctuations are sufficiently large that for no orientation does ''pure'' quasifission or fusion-fission occur, but only their probability changes with orientation of the target.

In the explanations considered, collisions with the sides of the target nuclei are more likely to result in the formation of fully equilibrated compound nuclei. For reactions with heavier projectiles, it may be only trajectories having favorable fluctuations from the average trajectory which can reach this configuration. The beam energy required to overcome the Coulomb barrier for this orientation is higher than that for the average barrier. The excitation energy of the compound nuclei will thus be higher, so whether the orientation dependence will act to enhance evaporation residue (E.R.) cross sections in such reactions depends on the variation with excitation energy of the survival probability of E.R.'s. This is sensitive to the excitation energy dependence of the fission width, which in turn is dependent on the dynamical fission time scale. A long dynamical fission time scale [26] will enhance E.R. survival for nuclei formed at relatively high excitation energy. The fact that very heavy elements have recently been formed [27] through the use of reactions on actinide targets, at bombarding energies above the average fusion barrier, is surely because of this interplay between the dynamics of fusion and fission.

Realistic modeling of the dynamical competition between fusion and quasifission, together with the fission-evaporation competition in the compound nuclei, should lead to a better understanding of the most favorable reactions and bombarding energies for very heavy and superheavy element production.

V. CONCLUSIONS

Fission fragment anisotropies and mass distributions have been measured to high accuracy, over a wide range of angles, for the $^{16}O + ^{238}U$ reaction. The bombarding energies spanned the fusion barrier distribution in fine energy steps. Fission following transfer reactions was rejected making use of the deduced velocity vectors of the fissioning nuclei, allowing precise determination of the properties of fission following full momentum transfer. The FMT fission cross sections allow extraction of the fusion barrier distribution, which shows that ^{238}U behaves in fusion as a prolate deformed nucleus, as expected.

The fission mass distributions for FMT fission show a small but significant skewness, which rises as the beam energy decreases through the fusion barrier region, displaying the same very characteristic energy dependence as the rise in fission fragment angular anisotropies. This is conclusive evidence in favor of the interpretation that collisions with the tips of the deformed ^{238}U target nuclei lead to quasifission, while collisions with the sides result in fusion-fission.

These experimental data show that a systematic deviation of the measured fission fragment anisotropies from the transition state model predictions appears to be the experimental quantity which is most sensitive to the presence of quasifission. It is also the most easily measured of the fission characteristics investigated in this experiment. These measurements confirm the validity of correlating anomalously large anisotropies with the presence of quasifission [3,12].

The above picture of the orientation dependence of the competition between quasifission and fusion-fission implies that true compound nucleus formation is suppressed at subbarrier energies, and enhanced at above-barrier energies, compared to expectations if the target were not deformed. There have been tentative theoretical suggestions (see for example Ref. [28]) that shape effects should be important in superheavy element formation reactions. This work proves conclusively that such shape effects play a major role in the dynamics of nuclear collisions with deformed heavy nuclei.

APPENDIX: KINEMATIC COINCIDENCE METHOD

The data analysis was based on the measured velocity vectors of the two fission fragments. This has been called the kinematic coincidence method [13]. The particular application of the method to this measurement is described here.

The velocity vectors of the fragments were defined in spherical polar coordinates, by scalar velocities v_i, the scattering angles θ_i, measured with respect to the beam direction, and the azimuthal angles ϕ_i, defined with respect to a convenient origin.

Initially, it is taken that the two velocity vectors and the beam axis are coplanar. As will be seen, this is equivalent to neglecting v_{perp}. This geometry is defined in Fig. 8(a). The velocities in the center-of-mass frame are denoted by V_i, while v_{par} represents the component in the beam direction of the center-of-mass velocity of the fissioning system. The measured velocity vectors can be decomposed into orthogonal components parallel and perpendicular to the beam axis. The former are given by $w_i = v_i \cos\theta_i$, the latter by $u_i = v_i \sin\theta_i$. Neglecting the small effects of prescission particle evaporation, the two fragments are taken as colinear in the center-of-mass frame, and the ratio

$$\frac{u_1}{u_2} = -\frac{w_1 - v_{\mathrm{par}}}{w_2 - v_{\mathrm{par}}}$$

can be defined, where the minus sign arises from the fact that u values (unlike w) can only be positive. Thus v_{par} is given in terms of the measured velocity components by

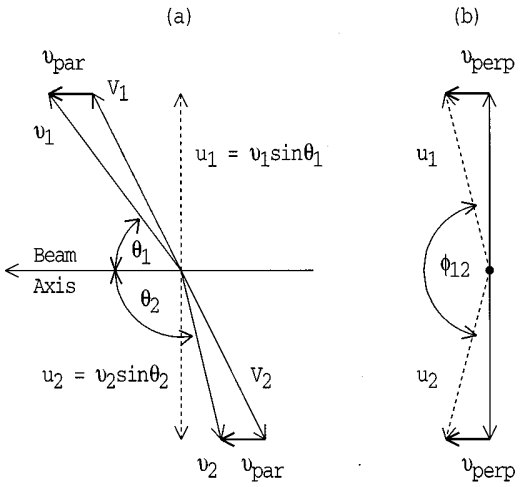

FIG. 8. Diagrams of the relevant fission fragment velocity components. Part (a) shows the plane including the fission fragment velocity vectors and the beam axis, while part (b) shows the plane perpendicular to the beam.

$$v_{\mathrm{par}}=\frac{u_1 w_2+u_2 w_1}{u_1+u_2}.$$

For fission following complete absorption of the projectile by the target, the full momentum of the projectile is transferred, and v_{par} should be equal to the calculated center-of-mass velocity for the collision $v_{\mathrm{c.m.}}$. However, as described in Sec. III A, deviations from binary kinematics due to emission of light particles perturbs the fission fragment vectors, resulting in a significant spread in v_{par} when the θ_i values are close to 0° and 180°. This can seriously affect the deduced mass split, if it is determined from momentum conservation in the plane *perpendicular* to the beam, using the equations

$$A_1 u_1=A_2 u_2, \quad M=\frac{u_1}{u_1+u_2}.$$

Here the A_i represent the masses of the two fragments, and M is the ratio of the fragment mass to the sum of the two fragment masses. To avoid this problem a different way of determining the mass split was used in the analysis. The fragment velocities in the center-of-mass frame V_i were evaluated taking v_{par} to be fixed at the value expected for complete fusion $v_{\mathrm{c.m.}}$. Then the mass split can be determined from the V_i by

$$M=\frac{V_1}{V_1+V_2}.$$

Thus accurate mass spectra could be determined at all angles for FMT fission, since as discussed in Sec. III A, the assumption that $v_{\mathrm{par}}=v_{\mathrm{c.m.}}$ is appropriate for FMT fission in these reactions.

Figure 8(b) shows the geometry in the plane perpendicular to the beam. The measured components u_i are related to the actual velocities of the fragments in the center-of-mass frame of the fissioning system by an in-plane vector having two components. The component parallel to the projection of the scission axis (solid lines in the figure) cannot be determined from the velocities alone. However that perpendicular to the scission axis can be, and is related to the azimuthal folding angle ϕ_{12}, as illustrated, and is denoted by v_{perp}. It is determined from the u_i and ϕ_{12} by the relationship

$$v_{\mathrm{perp}}=\frac{u_1 u_2 \sin\phi_{12}}{\sqrt{u_1^2+u_2^2-2u_1u_2\cos\phi_{12}}}.$$

For FMT fission, it is only light particle emission which causes v_{perp} to deviate from zero, so the deviation is small. Thus the u_i are very close to the actual fragment velocities [see Fig. 8(b)], so the assumption of planar geometry used in the derivation of M is completely acceptable. For fission following a transfer reaction, v_{perp} can be much larger, and is related to the center-of-mass velocity of the reaction. If v_{perp} is not small compared to the u_i, as it may be for transfer fission, the kinematic coincidence method must be used with caution, since binary kinematics are no longer appropriate.

[1] T. Murakami, C.-C. Sahm, R. Vandenbosch, D.D. Leach, A. Ray, and M.J. Murphy, Phys. Rev. C **34**, 1353 (1986).
[2] H. Zhang, Z. Liu, J. Xu, X. Quian, Y. Qiao, C. Lin, and K. Xu, Phys. Rev. C **49**, 926 (1994), and references therein.
[3] D.J. Hinde, M. Dasgupta, J.R. Leigh, J.P. Lestone, J.C. Mein, C.R. Morton, J.O. Newton, and H. Timmers, Phys. Rev. Lett. **74**, 1295 (1995).
[4] N. Majumdar, P. Bhattacharya, D.C. Biswas, R.K. Choudhury, D.M. Nadkarni, and A. Saxena, Phys. Rev. C **51**, 3109 (1995).
[5] A. Karnik, S. Kailas, A. Chatterjee, P. Singh, A. Navin, D.C. Biswas, D.M. Nadkarni, A. Shrivastava, and S.S. Kapoor, Z. Phys. A **351**, 195 (1995).
[6] R. Vandenbosch and J.R. Huizenga, *Nuclear Fission* (Academic, New York, 1973).
[7] R. Vandenbosch, Annu. Rev. Nucl. Part. Sci. **42,** 447 (1992).
[8] C.R. Morton, D.J. Hinde, J.R. Leigh, J.P. Lestone, M. Dasgupta, J.C. Mein, J.O. Newton, and H. Timmers, Phys. Rev. C **52**, 243 (1995).
[9] V.S. Ramamurthy and S.S. Kapoor, Phys. Rev. Lett. **54**, 178 (1985).
[10] Z.H. Liu, H.Q. Zhang, J.C. Xu, Y. Qiao, and C.J. Lin, Phys. Lett. B **353**, 173 (1995).
[11] D. Vorkapić and B. Ivanišević, Phys. Rev. C **52**, 1980 (1995).
[12] B.B. Back, R.R. Betts, J.E. Gindler, B.D. Wilkins, S. Saini, M.B. Tsang, C.K. Gelbke, W.G. Lynch, M.A. McMahan, and P.A. Baisden, Phys. Rev. C **32**, 195 (1985).
[13] J. Tōke, R. Bock, G.X. Dai, A. Gobbi, S. Gralla, K.D. Hildenbrand, J. Kuzminski, W.J.F. Müller, A. Olmi, and H. Stelzer, Nucl. Phys. **A440**, 327 (1985).
[14] N. Shinohara, S. Usuda, S. Ichikawa, T. Suzuki, M. Magara, H.

Okashita, H. Yoshikawa, T. Horiguchi, Y. Iwata, S. Shibata, and I. Fujiwara, Phys. Rev. C **34**, 909 (1986).
[15] N. Rowley, G.R. Satchler, and P.H. Stelson, Phys. Lett. B **254,** 25 (1991).
[16] J.X. Wei, J.R. Leigh, D.J. Hinde, J.O. Newton, R.C. Lemmon, S. Elfström, and J.X. Chen, Phys. Rev. Lett. **67**, 3368 (1991).
[17] J.R. Leigh, N. Rowley, R.C. Lemmon, D.J. Hinde, J.O. Newton, J.X. Wei, J.C. Mein, C.R. Morton, S. Kuyucak, and A.T. Kruppa, Phys. Rev. C **47**, R437 (1993).
[18] M. Dasgupta, A. Navin, Y.K. Agarwal, C.V.K. Baba, H.C. Jain, M.L. Jhingan, and A. Roy, Nucl. Phys. **A539**, 351 (1992).
[19] E.N. Shurshikov, Nucl. Data Sheets **53**, 601 (1988).
[20] D.J. Hinde, C.R. Morton, M. Dasgupta, J.R. Leigh, J.C. Mein, and H. Timmers, Nucl. Phys. **A592**, 271 (1995).
[21] M.G. Itkis, Yu.Ts. Oganessian, G.G. Chubarian, V.S. Salamatin, A.Ya. Rusanov, and V.N. Okolovich, in *Proceedings of the Low Energy Nuclear Dynamics Conference,* St. Petersburg, Russia, April 18–22, 1995, edited by Yu. Oganessian, W. von Oertzen, and R. Kalpakchieva (World Scientific, Singapore, 1995), p. 177.
[22] J.P. Lestone, Phys. Rev. C **51**, 580 (1995).
[23] D.J. Hinde, J.R. Leigh, J.J.M. Bokhorst, J.O. Newton, R.L. Walsh, and J.E. Boldeman, Nucl. Phys. **A472**, 318 (1987).
[24] K.T.R. Davies and A.J. Sierk, Phys. Rev. C **31,** 915 (1985).
[25] V.S. Ramamurthy, S.S. Kapoor, R.K. Choudhury, A. Saxena, D.M. Nadkarni, A.K. Mohanty, B.K. Nayak, S.V. Sastry, S. Kailas, A. Chatterjee, P. Singh, and A. Navin, Phys. Rev. Lett. **65**, 25 (1990).
[26] D.J. Hinde, D. Hilscher, H. Rossner, B. Gebauer, M. Lehmann, and M. Wilpert, Phys. Rev. C **45**, 1229 (1992).
[27] Yu.A. Lazarev, Yu.V. Lobanov, Yu.Ts. Oganessian, Yu.S. Tsyganov, V.K. Utyonkov, F.Sh. Abdullin, S. Iliev, A.N. Polyakov, J. Rigol, I.V. Shirokovsky, V.G. Subbotin, A.M. Sukhov, G.V. Buklanov, B.N. Gikal, V.B. Kutner, A.N. Mezentsev, I.M. Sedykh, D.V. Vakatov, R.W. Lougheed, J.F. Wild, K.J. Moody, and E.K. Hulet, Phys. Rev. Lett. **75**, 1903 (1995), and references therein.
[28] P. Möller and A. Iwamoto, Nucl. Phys. **A575**, 381 (1994).